AIAA 81-0001R

Particle Dynamics of Inlet Flowfields with Swirling Vanes

A. Hamed*
University of Cincinnati, Cincinnati, Ohio

The particle trajectories are investigated for the inlet flowfield of a helicopter engine with swirling vanes and particle separator. The flowfield resulting from the swirling vanes is first computed on a hub-shroud midchannel stream surface. The trajectories of the solid particles are then determined in this flowfield, including particle impacts with the hub, tip, and vane surfaces. The particle rebounding velocity and direction after each impact is determined using empirical correlations derived from experiments conducted in a special tunnel. Different particle sizes are considered, and the resulting trajectories and separator effectiveness are presented.

Nomenclature

B = tangential space between blades
C_p = specific heat at constant pressure
F = vector normal to midchannel stream surface and proportional to tangential pressure gradient
H = stagnation enthalpy
N = unit vector normal to the vane, hub, or tip
p = stagnation pressure
R = gas constant
r = radial distance from the axis
r_c = radius of curvature of meridional streamline
S = entropy
s = distance along orthogonal mesh lines in through-flow direction
T = temperature
t = distance along orthogonal mesh lines in direction across flow
T = unit vector tangent to the vane, hub, or tip
u = normalized stream function
V = flow velocity
V_p = particle velocity
z = axial coordinate
α = angle between meridional streamline and axial direction
β = angle between flow velocity vector and meridional plane
β_I = angle between impacting particle velocity and the surface
θ = angular coordinate
ρ = gas density
ρ_p = particle density
τ = time
ϕ = angle between s line and axial direction

Subscripts

i = inlet conditions
m = component in direction of meridional streamline
N = component normal to vane, hub, or tip surface
p = particle
r = component in radial direction
s = component in s direction
t = component in t direction
T = component tangent to vane, hub, or tip surface
z = component in axial direction
θ = component in tangential direction

Presented as Paper 81-0001 at the AIAA 19th Aerospace Sciences Meeting, St. Louis, Mo., Jan. 12-15, 1981; submitted Feb. 19, 1981; revision received Jan. 4, 1982.

*Professor, Department of Aerospace Engineering and Applied Mechanics. Member AIAA.

Introduction

MANY gas turbine engines operate in environments where the ingestion of solid particles is inevitable. In aircraft and naval installations the particles encountered can be sand, dust, or salt. Solid particles are also ingested by gas turbine engines in ground vehicles, auxiliary power units, and tanks. Continued operation under these conditions adversely affects the performance of these engines, as well as their life, and can be detrimental to their reliability. Engine inlet separators have been used to protect the jet engine components from the erosion caused by the solid particles. These separators eliminate most or some of the ingested particles from the engine's mainstream. Depending on the application, the separators can range from complex designs to simple scrolls for scavenging the ingested particles. An integrated inlet separator for the G.E. T700 helicopter gas turbine engine was described in Ref. 1. The design of this separator combines the swirling flowfield action produced by the inlet swirling vanes with the reflecting action of a hump shaped annulus hub. Both effects act to deflect the particles radially in order to be collected at the scroll inlet.

It is very important to be able to calculate the effectiveness of these devices if one is to determine the influence of the remaining particles on the engine life and performance. The particle trajectories in the inlet separators provide this information, in addition to the initial conditions for the subsequent trajectories of the unseparated particles through the gas turbine engine. The intensity and pattern of the compressor and turbine erosion is dependent on these initial conditions and on the separator effectiveness.

The most widely used code for the three-dimensional particle trajectory calculations through turbines and compressors was developed by Hussein and Tabakoff.[2] This code has been used extensively in axial flow compressor and turbine stages,[3,4] where the hub and tip radii do not change considerably within the blade row. The success of this code is attributed to its accurate representation of the blade airfoil shape and the blade-to-blade flowfield at the mean radius. This code is not suited, however, for particle trajectory calculations in inlet flowfields, which are characterized by significant hub and tip contouring. It can be seen from Fig. 1 that the hub and tip geometries of the G.E. T700 integrated inlet separator are highly contoured. The hub is hump shaped before leading to the deswirling vanes preceding the compressor. The increase in the hub diameter, through the swirling vanes, which prevails from the engine inlet to the hump, helps to deflect the impacting particles in the radial direction. On the other hand, the tip diameter is increased gradually starting near the trailing edge of the swirling vanes, to guide the scavenged flow. This configuration also helps to reduce the possibility of particles reentering the engine after

impacting the tip in this region. It can also be seen from Fig. 1, that the vanes have a considerable twist to produce a near free vortex circumferential velocity distribution and to impart larger tangential velocities to the impacting particles near the hub. Since the code of Ref. 2 is based on a flowfield solution at the mean radius, it will not represent the variation of the flowfield and the vane shape in the radial direction.

Other existing studies[5,6] of the particle trajectories in analytically prescribed flowfields do not include the effect of impacts with the solid boundaries. Particle impacts and subsequent rebounds with the tip and the swirling vanes have not been included in the calculations of Fabian and Oates[7] for the particle trajectories in the G.E. T700 integrated jet engine separator. These impacts will be shown to have a significant effect on the particle trajectories. The impacts with the vane's concave surface leads to their consequent separation by centrifugion. It will also be shown that the influence of the particles' impacts with the separator's outer annulus wall is very important, since they cause larger particles to reenter the engine's mainstream.

In this paper the author presents a new method for particle trajectory calculations. It includes the influence of the hub and tip shapes, as well as the radial variations in the flowfield, and the vane shape on the particle trajectories. The particle impacts with the vanes and with the inner and outer annuli are accurately represented in the three-dimensional particle trajectory calculations. The code has been used to determine the particle dynamics in the G.E. T700 helicopter gas turbine engine integrated inlet separator. The computed trajectories are presented for different particle sizes ranging between 5 and 1000 μ in diameter. The results are discussed to explain the influence of the hub, tip, and swirling vane impacts on the trajectory and separation of the different particle sizes.

Analysis

The particle dynamics in a gas solid suspension are determined by the gas-particle interaction and particle-boundary impacts. For the small particle concentrations, the particle-particle interactions are not significant and the flowfield is not affected by the presence of the particles. In the trajectory calculations, the equations governing the particle motion in the gas flowfield are integrated numerically and the location of their impacts with the various boundaries are determined. The particle rebounding velocity after each impact depends on the magnitude and direction of the impacting velocity, relative to the surface. The accurate representation of the flowfield, and of the geometry of the various boundaries, is essential to the success of any trajectory calculations.

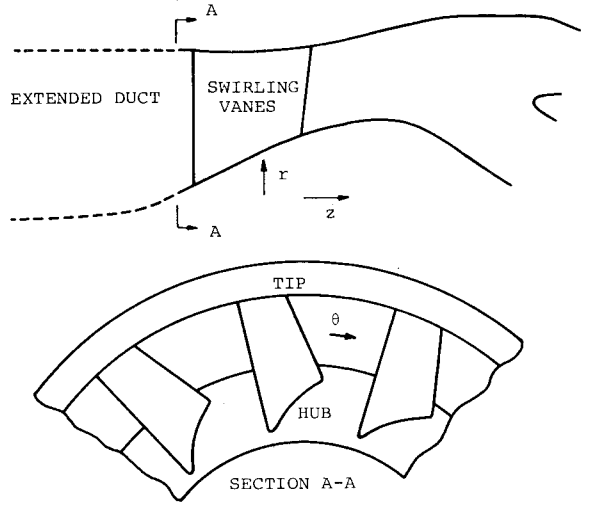

Fig. 1 Schematic inlet separator.

Flowfield

The three-dimensional flowfield through the engine inlet with swirling vanes is very complex. It has been traditional in turbomachinery flow computations to divide the problem into two, two-dimensional flow solutions, on blade-to-blade, and hub-tip stream surfaces.[8] The meridional solution is usually chosen when significant variations in the flow properties exist in the radial direction, or when the axial variations in the hub and tip contours are significant. In the present analysis, the flowfield solution was obtained on a midchannel hub-tip stream surface. This surface has the same shape as the blade mean camber, except near the leading and trailing edges, where corrections are made to match the freestream flow.

The flow computations were performed using the code of Ref. 9. This program combines the finite-difference method, which is used to obtain subsonic flow solutions, with the velocity gradient method, which extends the range to transonic flowfields. This code has been modified to provide output data appropriate for particle trajectory calculations.

Governing Equations

The subsonic flow analysis is based on the stream function formulation. Referring to Fig. 2, the momentum equation in the t direction is given by[9]

$$-\frac{V_\theta}{r}\frac{\partial(rV_\theta)}{\partial t}+V_s\left(\frac{\partial V_t}{\partial s}-\frac{\partial V_s}{\partial t}+V_s\frac{\partial\phi}{\partial s}+V_t\frac{\partial\phi}{\partial t}\right)$$
$$=-\frac{\partial H}{\partial t}+T\frac{\partial S}{\partial t}+F_t \tag{1}$$

where s and t are the distance along an orthogonal mesh, with s in the streamwise direction and t normal to it, and ϕ is the angle between s and the axial direction.

The velocity components V_s and V_t can be expressed in terms of the derivatives of the normalized stream function u as follows:

$$\frac{\partial u}{\partial s}=-\frac{rB\rho}{G}V_t \tag{2}$$

$$\frac{\partial u}{\partial t}=-\frac{rB\rho}{G}V_s \tag{3}$$

where B represents the stream-filament thickness, which is taken as the overall blade-to-blade spacing, and G is the mass flow through one blade channel.

Substituting Eqs. (2) and (3) into Eq. (1) and using the energy equation and the equation of state, one obtains

$$\frac{\partial^2 u}{\partial s^2}+\frac{\partial^2 u}{\partial t^2}-\frac{\partial u}{\partial s}\left(\frac{\sin\phi}{r}+\frac{1}{B}\frac{\partial B}{\partial t}+\frac{1}{\rho}\frac{\partial\rho}{\partial s}+\frac{\partial\phi}{\partial t}\right)$$
$$-\frac{\partial u}{\partial t}\left(\frac{\cos\phi}{r}+\frac{1}{B}\frac{\partial B}{\partial t}+\frac{1}{\rho}\frac{\partial\rho}{\partial t}+\frac{\partial\phi}{\partial s}\right)$$
$$+\frac{rB\rho}{GV_s}\left[\frac{V_\theta}{r}\frac{\partial(rV_\theta)}{\partial t}+\xi V^2+\zeta+F_t\right]=0 \tag{4}$$

where

$$\xi=\frac{1}{2}\left(\frac{R}{C_p p}\frac{\partial p}{\partial t}-\frac{1}{H}\frac{\partial H}{\partial t}\right) \tag{5}$$

$$\zeta=-\frac{HR}{pC_p}\frac{\partial p}{\partial t} \tag{6}$$

All the partial derivatives with respect to s and t in the above equations represent the derivatives on the midchannel stream surface shown in Fig. 2. The force component, F_t, is caused by the hub-tip pressure gradient induced by the blades. It is therefore equal to zero outside the blade passage and is calculated from the following relation inside the blade

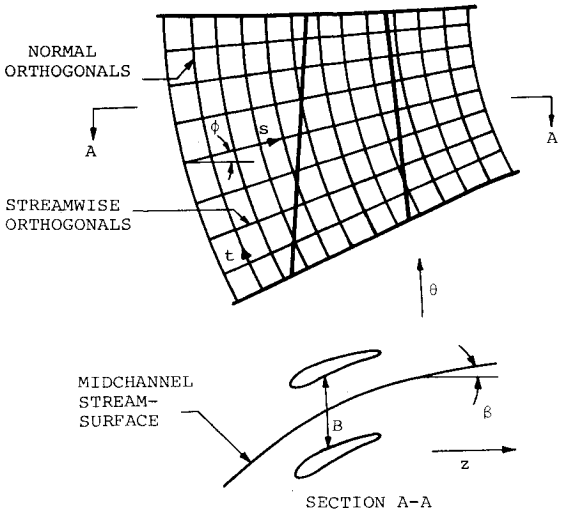

Fig. 2 Stream surface and orthogonal mesh.

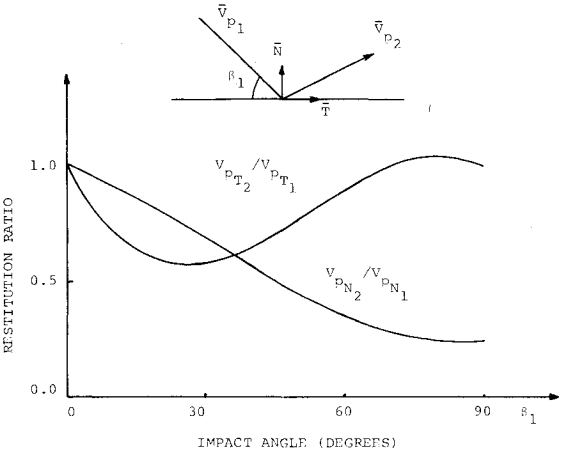

Fig. 3 Particle rebound characteristics.

passage:

$$F_t = -\frac{\partial \theta}{\partial t} V \frac{\partial V}{\partial \theta} \tag{7}$$

The stream function calculations are performed using an orthogonal grid which is generated using the method of Ref. 10. Two levels of iterations are used in the solution of the resulting equations. The solution of the linearized finite-difference equations is obtained using successive overrelaxation, and the corrections to the nonlinear terms are performed in the outer iterations. The values of the normalized stream function are specified to be zero at the hub and 1 at the tip. On the upstream and downstream boundaries, the derivative of the stream function normal to the boundary is assumed to be zero. This implies that the upstream and downstream boundaries must be orthogonal to the streamlines. After the stream function solution is obtained, the velocity components V_s and V_t are calculated according to Eqs. (2) and (3). The velocity components in the cylindrical polar coordinates are calculated using the following relations:

$$V_z = V_s \cos\phi - V_t \sin\phi \tag{8}$$

$$V_r = V_t \cos\phi + V_s \sin\phi \tag{9}$$

$$V_\theta = \tan\beta (V_s^2 + V_t^2)^{1/2} \tag{10}$$

where β is the angle between the flow velocity vector and the meridional plane.

The transonic flow solutions are obtained using the velocity gradient method. These solutions are based on the integration of the following velocity gradient equation in the t direction[9]:

$$\frac{dV}{dt} = V\left[\frac{\cos^2\beta + \cos(\alpha-\phi)}{r_c} - \frac{\sin^2\beta\cos\phi}{r} + \sin\alpha\sin\beta\cos\beta\frac{d\theta}{dt}\right] + \cos\beta\frac{dV_m}{dt}\sin(\alpha-\phi) + r\cos\beta\frac{dV_\theta}{dm}\frac{d\theta}{dt} + \frac{I}{V}\left[\frac{d(H_i - H)}{dt} - \xi - V^2\xi\right] \tag{11}$$

where

$$V_m = (V_s^2 + V_t^2)^{1/2} \tag{12}$$

The angle β is known only inside the blade channel. Outside the blade channel, it is eliminated using the relation

$$\sin\beta = V_\theta / V \tag{13}$$

The solutions to the velocity gradient equations for transonic flow are based on the information from the finite-difference solution at a reduced mass flow rate.

Flowfield Computations

The core and scavenged flowfields were calculated separately, using iterations to adjust the dividing streamline by trial and error. In performing the flow computations, the duct was extended upstream as shown by the dotted lines in Fig. 3, and uniform axial flow conditions were imposed at the inlet of the extended duct. The computations were performed using a 40×8 grid for the core engine flow and a 40×4 grid for the scavenged flow. The input for the twisted vane geometrical data was specified at the hub and tip, where the stagger angles are 30.1 and 22.5 deg, respectively.

Particle Dynamics

For the inlet flowfield, the drag represents the only force of interaction between the two phases. The particle collisions and the gravity force are not included because of their insignificant effects on the particle dynamics in the engine inlet separator. Under these conditions the equations governing the particle motion are written in cylindrical polar coordinates as follows:

$$\frac{d^2 r_p}{d\tau^2} = F\left(V_r - \frac{dr_p}{d\tau}\right) + r\left(\frac{d\theta_p}{d\tau}\right)^2 \tag{14}$$

$$r\frac{d^2\theta_p}{d\tau^2} = F\left(V_\theta - r\frac{d\theta_p}{d\tau}\right) - 2\frac{dr_p}{d\tau}\frac{d\theta_p}{d\tau} \tag{15}$$

$$\frac{d^2 z_p}{d\tau^2} = F\left(V_z - \frac{dz_p}{d\tau}\right) \tag{16}$$

where r_p, θ_p, and z_p define the particle location in cylindrical polar coordinates, and V_r, V_θ, V_z represent gas velocities in the radial, circumferential, and axial directions, respectively. The centrifugal force and Coriolis acceleration are represented by the last terms on the right-hand side of Eqs. (14) and (15). The force of interaction between the two phases per unit mass of particles is represented by the first term on the right-hand side of Eqs. (14-16). It is dependent on the relative velocity between the particles and the gas flow, as well as the particle size and shape.

In the trajectory calculations the particles are assumed to be spherical, leading to the following expression for the interaction force parameter:

$$F = \frac{3}{4}\frac{\rho}{\rho_p}\frac{C_D}{d}\left[\left(V_r - \frac{dr_p}{d\tau}\right)^2 + \left(V_\theta - \frac{d\theta_p}{d\tau}\right)^2 + \left(V_z - \frac{dz_p}{d\tau}\right)^2\right]^{1/2} \tag{17}$$

where ρ, ρ_p are the gas and solid particle densities, respectively, d is the particle diameter, and C_D is the drag coefficient. The drag coefficient is dependent on the Reynolds number, which is based on the relative velocity between the particle and the gas. Empirical relations (3) are used to fit the drag curve over a wide range of Reynolds numbers.

Particle Impacts with the Solid Boundaries

After impacting a solid boundary, the magnitude and direction of the particle rebounding velocity is dependent on the particle material, the surface material, and on the impact conditions. Extensive experimental measurements of the particle rebound characteristics were obtained using high speed photography.[11,12] These experimental studies were carried out in special erosion tunnels, which were designed to include the aerodynamic effects in the rebound characteristics. The following empirical relations[11] for the rebound-to-impact restitution ratios were used in the trajectory calculations:

$$V_{p_{2_T}}/V_{p_{1_T}} = 1.0 - 2.12\beta_1 + 3.0775\beta_1^2 - 1.1\beta_1^3 \quad (18)$$

$$V_{p_{2_N}}/V_{p_{1_N}} = 1.0 - 0.4159\beta_1 - 0.4994\beta_1^2 + 0.292\beta_1^3 \quad (19)$$

Referring to Fig. 4, V_{p_N} and V_{p_T} represent the particle velocity components normal and tangent to the solid surface, and the subscripts *1* and *2* refer to the conditions before and after impact, respectively. In the above equations, β_1 is the angle between the impact velocity and the tangent to the surface in radians.

Trajectory Calculations

The particle trajectory calculations consist of the numerical integration of Eqs. (1-4) in the inlet flowfield. During the computations, the flow velocity and density are usually required at points within the orthogonal mesh. These values are computed from the grid point values using linear interpolation. The geometrical boundaries are defined by the (r,z) coordinates of the grid points at the inner and outer radii. The vane shapes are described by the θ coordinates at the grid points of the orthogonal mesh, and by the blade-to-blade passage width in the θ direction. Linear interpolation is used for the determination of the blade surface coordinates at other points.

For the specified initial conditions, the particle trajectory calculations proceed using a fixed time step in the numerical integration of Eqs. (14-17). The time step is reduced iteratively preceding particle impacts, to determine the impact location and the magnitude and direction of impact velocity. The rebounding velocity is then determined according to the empirical correlations of Eqs. (18) and (19). These correlations were simulated in a three-dimensional form to account for the three velocity components, and the twisted blade surfaces. The data describing the surface near the impact location are used to determine the unit vector N in the direction of the local outward normal to the surface.

Referring to Fig. 3, the impacting velocity components in the directions normal, and tangent to the surface, are calculated from the following relations:

$$V_{p_{1_N}} = -V_{p_1} \cdot N$$

and

$$V_{p_{1_T}} = -V_{p_1} \cdot T \quad (20)$$

where

$$T = \frac{N \times V_1 \times N}{|V_1|} \quad (21)$$

Knowing the rebounding velocity components V_{p2_N}, V_{p2_T} and the direction cosines of the unit vectors N and T, the rebounding velocity components are determined in the cylindrical polar coordinates. The impact locations and rebounding velocities constitute the initial conditions for the subsequent particle trajectory calculations. It is assumed in this analysis that the particles are not shattered by impacts.

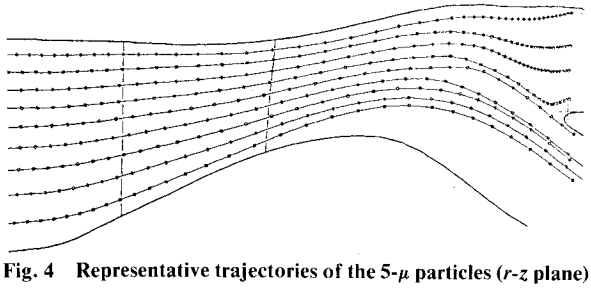

Fig. 4 Representative trajectories of the 5-μ particles (r-z plane).

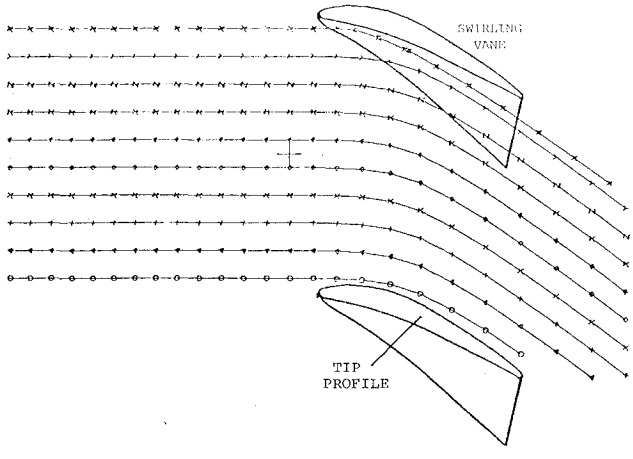

Fig. 5 Representative trajectories of the 5-μ particles (z-θ plane).

Results and Discussion

The particle trajectory calculations have been performed for various particle sizes ranging from 5 to 1000 μ in diameter. The trajectories are reported for particles which are introduced at several inlet radial locations, corresponding to intervals of 0.1 of the total mass flow rate. Sets of ten particles were introduced at each of these locations in the blade-to-blade channel. This distribution was chosen in order to easily interpret the results in terms of the percentage of particles separated. A time step of 0.0001 s was used in all the trajectory calculations except preceding impacts. The particles' initial velocities are taken equal to the gas flow velocity at their initial locations. The results are presented for various particle sizes to illustrate the generally different trajectory characteristics through the range of particle sizes. The projection of the trajectories on the r-z plane shows the particle radial migration and reveals whether the particles are separated or ingested. The projection of the trajectories on the z-θ plane shows the particle motion in the circumferential direction under the effect of the swirling flowfield and/or vane impacts.

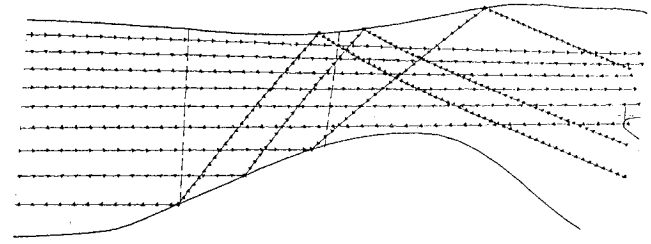

Fig. 6 Representative trajectories of 500-μ particles not impacting the vanes.

Table 1 Effect of particle size on the G.E. T700 separator effectiveness

Particle size, μ	Percentage separated owing to vane impacts	Percentage separated owing to hub impacts	Percentage separated without impacts	Overall separator effectiveness, %
5	4	0	51	55
10	18	10	71	99
20	23	18	58	99
50	27	25	47	99
100	32	30	36	98
200	34	17	39	90
500	23	5	38	66
1000	22	5	34	61

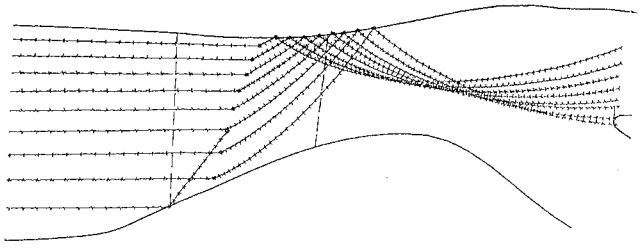

Fig. 7 Representative trajectories of 500-μ particles impacting the vanes.

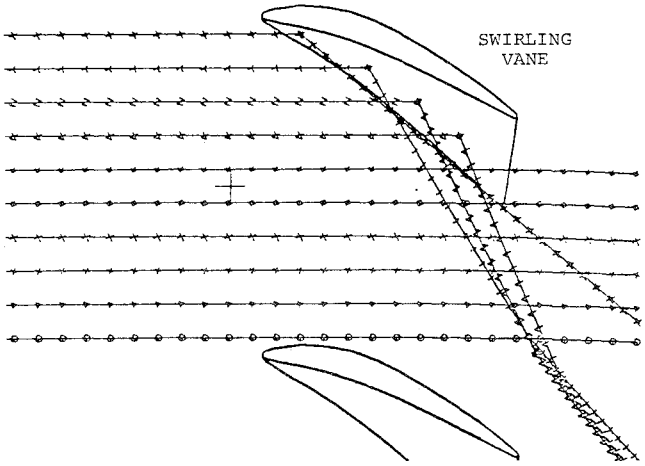

Fig. 8 Representative trajectories of 500-μ particles.

Some representative particle trajectories are presented for very small (5-μ) and very large (500-μ) particles. It can be seen from Fig. 4 that the small particles do not impact the hub or tip annulus, and that their radial migration increases after passing through the swirling vanes. Figure 5 shows that these small particles easily acquire a circumferential velocity component from the swirling flowfield which causes their centrifugion. Very few of these particles impact the vanes near the leading edge. It can generally be observed however that these vane impacts do not lead to a significant difference in the trajectory pattern of these particles. One can conclude, therefore, that neither hub nor vane impacts constitute a mechanism for the separation of the small particles. The centrifugion by the swirling flow is the main cause of small particle separation.

The representative trajectories of the 500-μ particles are shown in Figs. 6-8. The large relaxation times of these particles are responsible for the reduction in the influence of the swirling flowfield on their trajectory. It can be seen from Figs. 6-8 that more of these larger particles impact the hub, tip, and swirling vanes. Furthermore, the trajectories of the particles impacting the solid boundaries are drastically different from the rest in that they are mainly dominated by these impacts and subsequent rebounds. It can be seen from Fig. 6 that many of the particles impacting the hub reenter the engine core flowfield after they impact the tip. This effect is present in the trajectories of all particles greater than 100 μ in diameter, and its influence increases with increased particle size. This results in a reduction in the separator effectiveness for particles larger than 100 μ in diameter. On the other hand, more of these large particles impact the vanes owing to their higher inertia. Furthermore, their impact angles are generally larger, resulting in larger circumferential rebounding velocity components, as can be seen in Fig. 8. Figure 7 demonstrates that the vane impacts constitute the major cause of separation for these large particles.

The effect of the various mechanisms on the separation of the different particle sizes are summarized in Table 1. It can be concluded from the data in this table that, the smaller particles are mainly separated through the influence of the flowfield on their trajectories. The effect of the flowfield on the particle trajectories decreases with increased particle size. In the meantime, the impacts with the contoured hub and with the vanes start to influence the particle trajectories, leading to their separation. All three effects combine to result in the highest separator effectiveness over a wide range of intermediate particle sizes. The separator effectiveness is reduced for very large particles, since they tend to reenter the core flowfield after tip impacts. The separator is also not effective for the smallest particles which follow the flowfield into the engine core.

Acknowledgments

The author would like to express her thanks to Dr. Ted Katsanis for providing his updated flowfield computational code. The author also wishes to thank Dr. James R. Patton and Dr. Donald F. Brunda for the engine data. This research work was sponsored by the Office of Naval Research under Contract N00014-78-C-0590.

References

[1] Yaffe, M., "T700 Aims at Low Combat Maintenance," *Aviation Week and Space Technology,* Vol. 100, No. 4, Jan. 1974, pp. 45-53.

[2] Hussein, M.F. and Tabakoff, W., "Computer Program for Calculations of Particle Trajectories Through a Rotating Cascade," University of Cincinnati, Cincinnati, Ohio, Tech. Rept. 76-47, May 1976.

[3] Hussein, M.F. and Tabakoff, W., "Computation and Plotting of Solid Particle Flow in Rotating Cascades," *Computers and Fluids,* Vol. 2, 1974, pp. 1-15.

[4] Hussein, M.F. and Tabakoff, W., "Dynamic Behavior of Solid Particles Suspended by Polluted Flow in a Turbine Stage," *Journal of Aircraft,* Vol. 10, July 1973, pp. 434-440.

[5]Kriebel, A.R., "Particle Trajectories in a Gas Centrifuge," *Journal of Basic Engineering,* Vol. 83, Part 2, Sept. 1961, pp. 333-340.

[6]Lapple, C.E. and Sheperd, C.B., "Calculation of Particle Trajectories," *Industrial and Engineering Chemistry,* Vol. 32, May 1940, pp. 605-617.

[7]Fabian, J.M. and Oates, G.C., "Analysis of Flows Within Particle Separators," ASME Paper 77-WA/FE-21, 1977.

[8]Wu, C.H., "A General Theory of Three-Dimensional Flow in Subsonic and Supersonic Turbomachines of Axial, Radial and Mixed-Flow Types," NACA TN-2604, 1952.

[9]Katsanis, T. and McNally, W.D., "Revised Fortran Program for Calculating Velocities and Streamlines on the Hub-Shroud Mid Channel Stream Surface of an Axial, Radial, or Mixed Flow Turbomachine or Annular Duct," Vols. 1 and 2, NASA TN D-8430 and NASA TN D-8431, 1977.

[10]McNally, W.D., "FORTRAN Program for Generating a Two-Dimensional Orthogonal Mesh Between Two Arbitrary Boundaries," NASA TN D-6766, 1972.

[11]Tabakoff, W. and Hamed, A., "Aerodynamic Effects on Erosion in Turbomachinery," JSME and ASME Paper 70, *Proceedings of the 1977 Joint Gas Turbine Congress,* Tokyo, Japan, May 1977, pp. 574-581.

[12]Tabakoff, W. and Wakeman, T., "Test Facility for Material Erosion at High Temperatures," *Erosion: Prevention and Useful Applications,* ASTM Publication STP 664, 1978, pp. 123-134.